nature photonics

LETTERS

PUBLISHED ONLINE: 19 SEPTEMBER 2016 | DOI: 10.1038/NPHOTON.2016.179

Quantum teleportation with independent sources and prior entanglement distribution over a network

Qi-Chao Sun[1,2,3], Ya-Li Mao[1,2], Si-Jing Chen[4], Wei Zhang[5], Yang-Fan Jiang[1,2], Yan-Bao Zhang[6], Wei-Jun Zhang[4], Shigehito Miki[7], Taro Yamashita[7], Hirotaka Terai[7], Xiao Jiang[1,2], Teng-Yun Chen[1,2], Li-Xing You[4], Xian-Feng Chen[3], Zhen Wang[4], Jing-Yun Fan[1,2], Qiang Zhang[1,2]* and Jian-Wei Pan[1,2]*

Quantum teleportation[1] faithfully transfers a quantum state between distant nodes in a network, which enables revolutionary information-processing applications[2–4]. This has motivated a tremendous amount of research activity[5–24]. However, in the past not a single quantum-teleportation experiment has been realized with independent quantum sources, entanglement distribution prior to the Bell-state measurement (BSM) and feedforward operation simultaneously, even in the laboratory environment. We take the challenge and report the construction of a 30 km optical-fibre-based quantum network distributed over a 12.5 km area. This network is robust against noise in the real world with active stabilization strategies, which allows us to realize quantum teleportation with all the ingredients simultaneously. Both the quantum-state and process-tomography measurements and an independent statistical hypothesis test confirm the quantum nature of the quantum teleportation over this network. Our experiment marks a critical step towards the realization of a global 'quantum internet' in the real world.

Quantum entanglement is at the heart of quantum mechanics. Bennett *et al.* found that quantum entanglement is the key to realize the dream of teleportation[1]. Quantum teleportation faithfully transfers the quantum state of a physical system, instead of the system itself, between distant nodes, which underlies the proposals of distributed quantum computing[2,25] and quantum-communication networks[3,4].

Figure 1 depicts a future quantum network. The central node hosts a quantum processor. It shares entanglement with many relay nodes, which constitute a star-topology structure. The end user accesses the central quantum processor by teleporting the quantum state to the central node via the nearby relay node. The relay nodes perform an entanglement distribution and BSM, and feedforward the measurement outcomes to the central processor. The structure may be replicated to form a larger network. The quantum network with distant nodes demands that each node has an independent quantum source. Therefore, a critical step in the roadmap towards realizing a global quantum network is to implement independent quantum sources, prior entanglement distribution[16,24] and active feedforward operation[18] simultaneously in a single experimental realization of quantum teleportation in the real world. This remains an experimental challenge because it requires the interference of independent photons as flying qubits from distant nodes in a quantum network with a high and stable quantum-interference visibility. To do that, one can eliminate the spectral and spatial distinguishability by applying spectral and spatial filtering. However, the real challenge is that the fluctuation of the effective length of the quantum channel[13] in the real world makes independent photons distinguishable at interference, which was not a concern in previous experiments that were performed locally in a stable laboratory environment[26,27]. To overcome the challenge, we developed a number of experimental techniques to stabilize the quantum channel; in particular, we use the error signal derived from the photon arrival time in the feedback loop to reduce the overall time jitter between independent photons of distant nodes to 6 ps, which is insignificant compared with the 110 ps coherence time of photons. As such, the quantum interference between independent photons from distant nodes in our system is robust for all degrees of freedom and our experiment runs continuously with high state fidelity for weeks without maintenance.

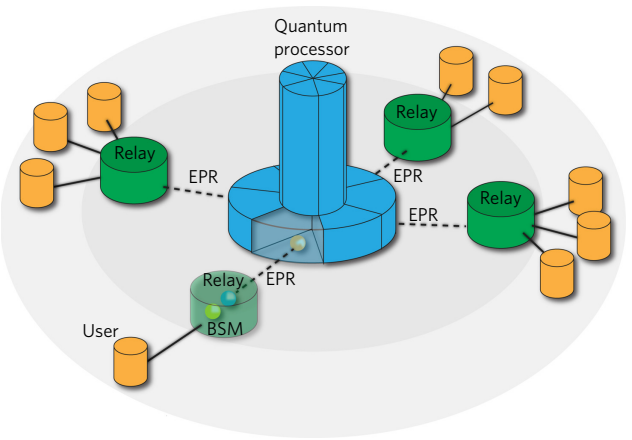

Figure 1 | Schematics of a quantum network with a star-topology structure. The central node hosts a quantum processor and shares entanglement with the relay nodes. The end users access the central quantum processor by teleporting the quantum states to the central node via the relay nodes. The relay nodes perform a BSM, and feedforward the measurement outcomes to the central processor.

[1]National Laboratory for Physical Sciences at Microscale and Department of Modern Physics, Shanghai Branch, University of Science and Technology of China, Shanghai 201315, China. [2]CAS Center for Excellence and Synergetic Innovation Center in Quantum Information and Quantum Physics, Shanghai Branch, University of Science and Technology of China, Shanghai 201315, China. [3]Department of Physics and Astronomy, Shanghai Jiao Tong University, Shanghai 200240, China. [4]State Key Laboratory of Functional Materials for Informatics, Shanghai Institute of Microsystem and Information Technology, Chinese Academy of Sciences, Shanghai 200050, China. [5]Tsinghua National Laboratory for Information Science and Technology, Department of Electronic Engineering, Tsinghua University, Beijing 100084, China. [6]Institute for Quantum Computing and Department of Physics and Astronomy, University of Waterloo, Waterloo, Ontario N2L 3G1, Canada. [7]Advanced ICT Research Institute, National Institute of Information and Communications Technology, 588-2, Iwaoka, Nishi-ku, Kobe, Hyogo 651-2492, Japan. *e-mail: qiangzh@ustc.edu.cn; pan@ustc.edu.cn

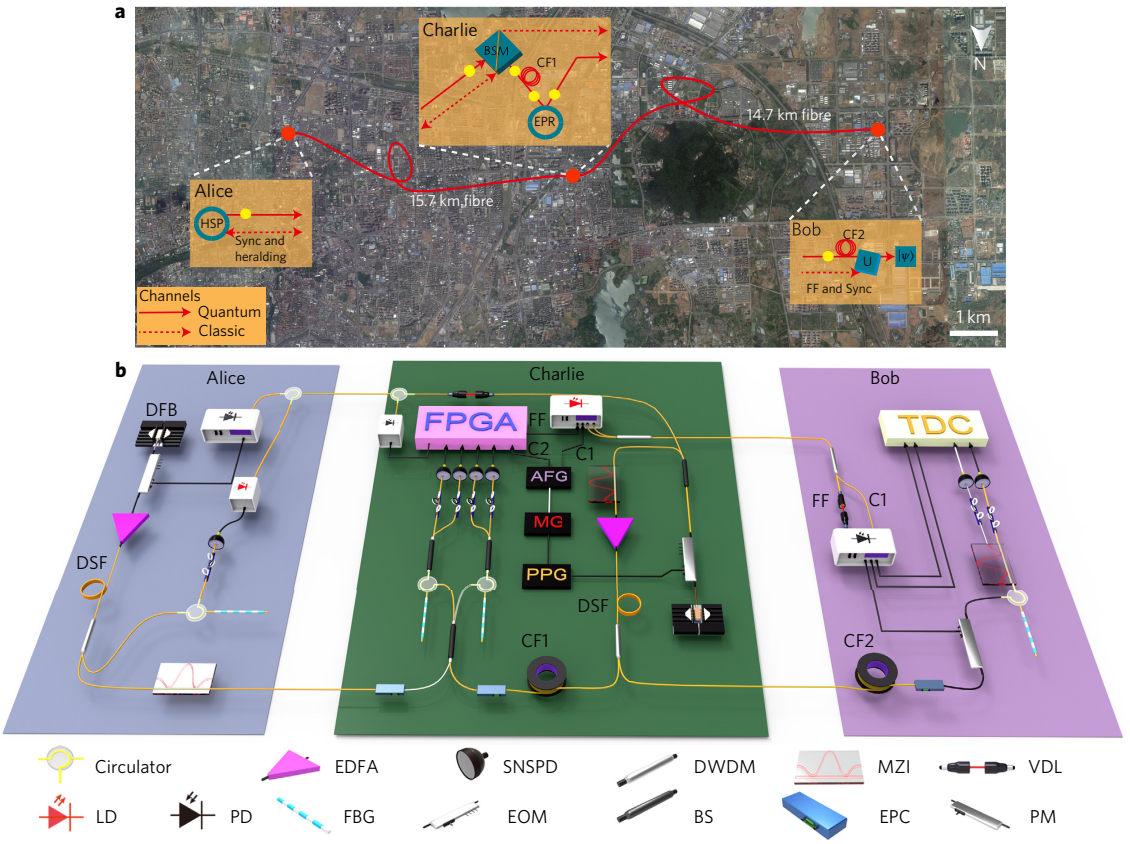

Figure 2 | Quantum teleportation in a Hefei optical fibre network. a, Bird's-eye view of the experiment. Alice prepares the quantum state, $|\psi\rangle_{in}$, on a heralded single photon (HSP) and sends it to Charlie, who shares an EPR pair with Bob beforehand. Each photon of the EPR pair is stored in a 15 km coiled fibre (CF). Charlie implements a BSM on his photon and the received HSP and then sends the feedforward signal to Bob, who performs a unitary correction operation (U) and state analysis. The quantum signals are transmitted in the optical fibre denoted by the solid line, whereas the classical signals are sent in another optical fibre denoted by the dashed line. **b**, Experimental set-up. Both Alice and Charlie generate photon pairs through the FWM process in the DSF. The MZIs are used in the state preparation and measurement (Methods). The microwave generator (MG) serves as master clock. To synchronize (Sync) the HSP source and EPR source, Charlie sends a portion of his pulse laser beam to Alice through an optical fibre channel, and Alice detects them by using a 45 GHz PD to generate driving pulses for an EOM. The heralding signals are converted into a laser pulses with a laser diode (LD) and transmitted to Charlie through the same optical fibre. Two optical circulators are used to achieve the bi-direction signal transmission. The feedforward signal (FF) and clock signals (C1, 10 MHz clock signal and C2, 200 MHz clock signal) generated by the arbitrary function generator (AFG) are carried by laser pulses with different wavelengths, which are launched into an optical fibre by a DWDM filter and sent to Bob. After being separated by another DWDM, the feedforward signal and 10 MHz clock are converted into electrical signals and fed to a time-to-digital converter (TDC). The feedforward signal is also used to trigger a short PG module to generate the driving pulse for the phase modulator (PM) to perform the unitary correction operation. Electronic-controlled polarization controllers (EPC) are used to compensate automatically the polarization drift caused by the optical fibre. Map data: Google. CNES/Astrium. DigitalGlobe.

To meet the requirement of prior entanglement distribution, we buffer EPR (Einstein, Podolsky, Rosen) photons in coiled optical fibre at both the relay node and the central node after entanglement distribution. This allows us to perform the BSM after the single photons arrive at the relay node and to forward the BSM outcomes in real time to the central node to do unitary transformation. Our quantum-teleportation experiment over a realistic network with independent quantum sources, prior entanglement distribution and active feedforward operation marks a critical step in the roadmap towards realizing a global quantum network.

The network is deployed in the city of Hefei, China. As shown in Fig. 2a, Charlie (N 31° 51′ 5.42″, E 117° 11′ 55.82″) is the relay, Alice (N 31° 50′ 7.50″, E 117° 15′ 50.56″) is the user and Bob (N 31° 50′ 11.42″, E 117° 7′ 54.37″) is the central processor. Alice (Bob) is connected to Charlie with a 15.7 km (14.7 km) single-mode optical fibre with a propagation loss of 5 dB (6 dB).

Figure 2b presents details of our experimental realization. Charlie prepares time-bin entangled pairs[28] of signal (s) and idler (i) photons in the quantum state of $|\Phi^+\rangle_{si} = 1/\sqrt{2}(|t_0\rangle_s|t_0\rangle_i + |t_1\rangle_s|t_1\rangle_i)$ at a repetition rate of 100 MHz via four-wave mixing (FWM), where $|t_0\rangle$ and $|t_1\rangle$ represent the first and second time bin, respectively (Methods). Charlie then sends the idler photon to Bob and holds the signal photon by propagating it in a 15 km coiled optical fibre. Similarly, Bob holds the idler photon after he receives it. The temporary storages allow us to perform a BSM after the entanglement distribution and implement the feedforward operation in real time. Alice generates correlated photon pairs similarly. She obtains single photons by heralding their idler partners and encodes the input quantum states $|\psi\rangle_{in} = \alpha|t_0\rangle_{in} + \beta|t_1\rangle_{in}$ onto the single photons. Both the encoded photons and their heralding signals (photodetection signal of the idler photons) are sent to Charlie.

Charlie passes the photons through a fibre Bragg grating (FBG) with a bandwidth of 4 GHz before the BSM, which is much smaller than the bandwidth of the pump pulse (8 GHz). After spectral filtering, the temporal coherence time of the single-photon pulse is about 110 ps, and the single-photon-state purity is measured to be 0.91 ± 0.03 and 0.84 ± 0.02 for photons from Alice and from Charlie, respectively, which approximate a single eigenmode in

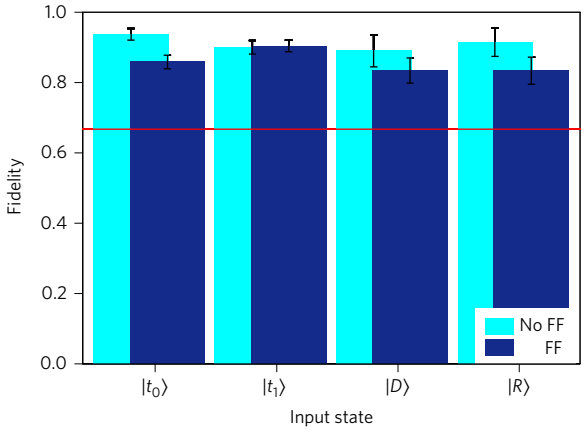

Figure 3 | State fidelities of quantum teleportation with four different input states: $|t_0\rangle$, $|t_1\rangle$, $|D\rangle$ and $|R\rangle$. The observed state fidelities without and with active feedforward operation are denoted by the colours cyan and blue, respectively. The error bars represent one standard deviation. All the observed state fidelities significantly exceed the classical fidelity limit of 2/3, represented by the red horizontal line.

the spectral domain. The use of single-mode optical fibre ensures the spatial indistinguishability. (FBGs are also used to reduce the bandwidth of idler photons.)

The long coherence time of the prepared quantum state allows us to synchronize independent quantum sources that are far apart with off-the-shelf instruments. We keep a master clock at the node of Charlie and use it to trigger a pulse-pattern generator (PPG). The PPG drives the electro-optic modulator (EOM) to carve the continuous wave (CW) laser beam periodically into 75 ps pulses, separated by 10 ns. These pulses are used to create the EPR pairs for Charlie after amplification. A fraction of each of these optical pulses is sent to Alice's side, where it is detected by a 45 GHz photodetector (PD). The photodetection signal is used to trigger the creation of Alice's quantum source. Although the quantum sources and BSM were within the same laboratory in previous experiments, in our field test the single photons need to travel through a fibre from Alice to Charlie, which are separated by 6.5 km in the field. The ambient temperature can change by more than 10 °C over 24 hours. As a result, the effective length and polarization property of the fibre change significantly, which can make the photons from separate sources distinguishable. We feed back the error signal derived from the photon-arrival time to the variable delay line (VDL) to control the creation of independent quantum sources. By reducing the time jitter between independent photons to 6 ps, we largely suppress the distinguishability. The change in fibre-polarization property can change the photon count rate by more than 100% in 70 hours of continuous measurement, which is reduced to 3% by using a separate feedback loop (Supplementary Section 3). It is evident that this method can be used to synchronize many nodes of a quantum network.

By using a fibre beamsplitter (BS) tree and four superconducting nanowire single photon detectors (SNSPDs), Charlie is able to discriminate the EPR state $|\Psi^-\rangle$ deterministically and the EPR state $|\Psi^+\rangle$ with 50% success (Methods). We use the field-programmable gate array (FPGA) to execute the feedforward logic based on the photodetection signals from the SNSPDs and the heralding signals from Alice. The FPGA sends a signal to Bob for each successful threefold coincidence detection. At Bob's side, he performs a unitary phase flip operation on the photon only if the signal from

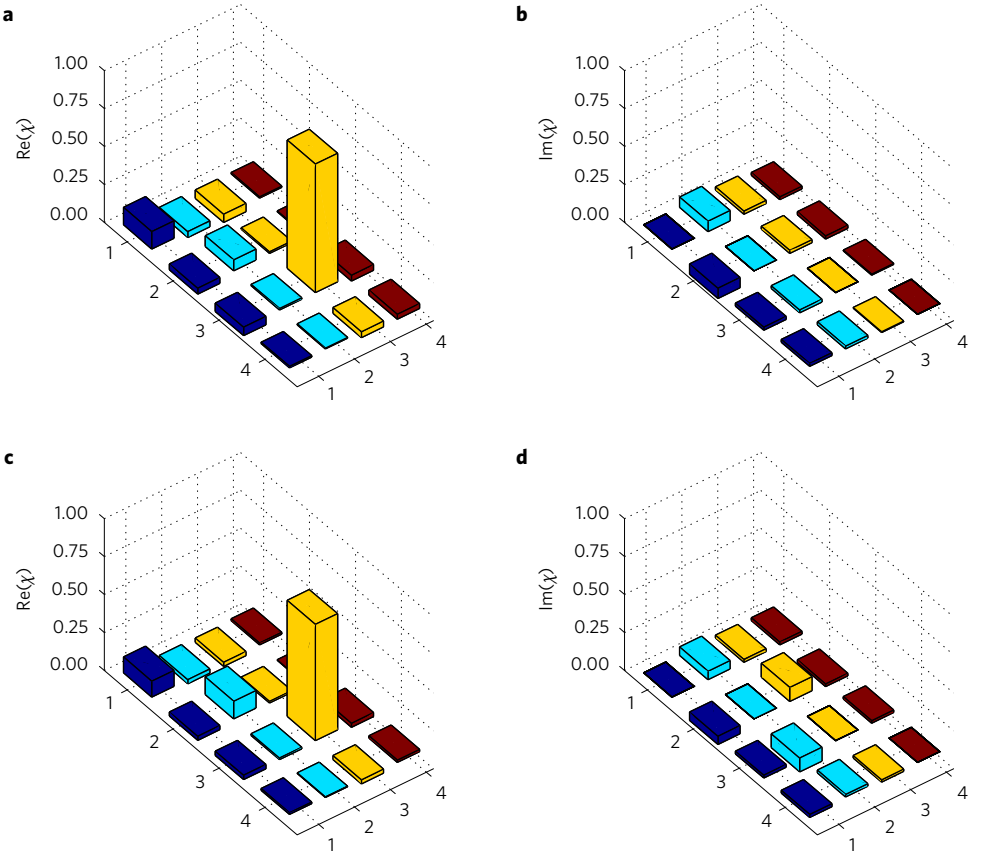

Figure 4 | Quantum-process tomography of quantum teleportation. a–d, Process matrices for quantum teleportation without (**a**,**b**) and with (**c**,**d**) active feedforward operation, respectively.

the FPGA corresponds to the Bell state $|\Psi^+\rangle$ in the BSM. Thus, the final state of the photon in Bob's possession is $|\psi\rangle_{\rm fin} = -\sigma_y|\psi\rangle_{\rm in}$. Feedback controls are used to optimize unitary transform on the single photon.

To characterize completely the field test of quantum teleportation, we perform quantum-state-tomography measurements[23] on the teleported quantum states. Without the loss of generality, we choose quantum states $|t_0\rangle$, $|t_1\rangle$, $|D\rangle$ and $|R\rangle$ as input states, where $|D\rangle = 1/\sqrt{2}(|t_0\rangle + |t_1\rangle)$ and $|R\rangle = 1/\sqrt{2}(|t_0\rangle + i|t_1\rangle)$. We reconstruct density matrices for teleported quantum states, with which we calculate the state fidelities, as shown in Fig. 3. The average quantum-state fidelities are 0.91 ± 0.02 and 0.85 ± 0.02 without feedforward operation (when the BSM outcome corresponds to the Bell state $|\Psi^-\rangle$) and with active feedforward operation (when the BSM outcome corresponds to either Bell state $|\Psi^-\rangle$ or $|\Psi^+\rangle$), both exceeding the classical limit of 2/3. The observed imperfections partly arise from multiphoton processes in the FWM and non-ideal unitary rotations. The lower state fidelity with a feedforward operation is mainly caused by the use of a low-bandwidth pulse generator (PG), which distorts the waveform in realizing the phase flip and will be improved in a future experiment. Following Nielsen and Chuang[2], we perform quantum-process-tomography measurements and determine the process matrices, which are shown in Fig. 4. The quantum-process fidelities for quantum teleportation in our field test are 0.84 ± 0.04 and 0.77 ± 0.03, respectively, for without active feedforward operation and for with active feedforward operation (Methods).

Lastly, we examine the possibility for any classical process to produce the results observed in our field test. In a classical teleportation, Charlie directly measures the input state and informs Bob to reconstruct the state accordingly, with a maximum state fidelity of 2/3. However, because of a finite number of experimental trials, the statistical fluctuation may allow the classical teleportation to reach and even exceed the state fidelity observed in our experiment. This is quantified by a probability according to Hoeffding's inequality[29]:

$$\mathrm{Prob}_{\rm classical}(\bar{F}_{\rm classical} \geq \bar{F}) \leq \left[\left(\frac{4/3 - 2/3}{4/3 - \bar{F}} \right)^{\frac{4/3-\bar{F}}{4/3}} \left(\frac{2/3}{\bar{F}} \right)^{\frac{\bar{F}}{4/3}} \right]^{4N} \quad (1)$$

where $\bar{F}$ is the state fidelity observed in the experiment and N is the number of experimental trials for each input quantum state. The above inequality reads as that the probability according to any classical process of predicting an average fidelity $\bar{F}_{\rm classical}$ no less than the observed average fidelity $\bar{F}$ is no more than the right-hand side of equation (1), which in our experiment is 1.5×10^{-16} with $N = 150$ for quantum teleportation without active feedforward or 2.4×10^{-14} with $N = 240$ for quantum teleportation with active feedforward. With these, we confirm the quantum nature of teleportation over the 30 km optical fibre network.

By applying a variety of feedback mechanisms to suppress the noise in wavelength, time, spectrum, phase, polarization and power, we realize a robust quantum-teleportation system in the real world. Our experiment, along with the two recent field tests of quantum teleportation[17,18], may serve as the benchmark to realize quantum teleportation in the real world. The developed technology is immediately applicable to a wide array of quantum information-processing applications with independent quantum sources.

During the writing and submission of this manuscript we became aware of the work by Valivarthi and colleagues[30].

Methods

Methods and any associated references are available in the online version of the paper.

Received 18 February 2016; accepted 9 August 2016; published online 19 September 2016

References

1. Bennett, C. H. *et al.* Teleporting an unknown quantum state via dual classical and Einstein–Podolsky–Rosen channels. *Phys. Rev. Lett.* **70,** 1895–1899 (1993).
2. Nielsen, M. A. & Chuang, I. L. *Quantum Computation and Quantum Information* (Cambridge Univ. Press, 2010).
3. Cirac, J. I., Zoller, P., Kimble, H. J. & Mabuchi, H. Quantum state transfer and entanglement distribution among distant nodes in a quantum network. *Phys. Rev. Lett.* **78,** 3221–3224 (1997).
4. Kimble, H. J. The quantum internet. *Nature* **453,** 1023–1030 (2008).
5. Bouwmeester, D. *et al.* Experimental quantum teleportation. *Nature* **390,** 575–579 (1997).
6. Boschi, D., Branca, S., De Martini, F., Hardy, L. & Popescu, S. Experimental realization of teleporting an unknown pure quantum state via dual classical and Einstein–Podolsky–Rosen channels. *Phys. Rev. Lett.* **80,** 1121–1125 (1998).
7. Furusawa, A. *et al.* Unconditional quantum teleportation. *Science* **282,** 706–709 (1998).
8. Nielsen, M. A., Knill, E. & Laflamme, R. Complete quantum teleportation using nuclear magnetic resonance. *Nature* **396,** 52–55 (1998).
9. Marcikic, I., de Riedmatten, H., Tittel, W., Zbinden, H. & Gisin, N. Long-distance teleportation of qubits at telecommunication wavelengths. *Nature* **421,** 509–513 (2003).
10. Ursin, R. *et al.* Communications: quantum teleportation across the Danube. *Nature* **430,** 849–849 (2004).
11. Barrett, M. *et al.* Deterministic quantum teleportation of atomic qubits. *Nature* **429,** 737–739 (2004).
12. Riebe, M. *et al.* Deterministic quantum teleportation with atoms. *Nature* **429,** 734–737 (2004).
13. de Riedmatten, H. *et al.* Long distance quantum teleportation in a quantum relay configuration. *Phys. Rev. Lett.* **92,** 047904 (2004).
14. Sherson, J. F. *et al.* Quantum teleportation between light and matter. *Nature* **443,** 557–560 (2006).
15. Zhang, Q. *et al.* Experimental quantum teleportation of a two-qubit composite system. *Nature Phys.* **2,** 678–682 (2006).
16. Landry, O., van Houwelingen, J. A. W., Beveratos, A., Zbinden, H. & Gisin, N. Quantum teleportation over the swisscom telecommunication network. *J. Opt. Soc. Am. B* **24,** 398–403 (2007).
17. Yin, J. *et al.* Quantum teleportation and entanglement distribution over 100-kilometre free-space channels. *Nature* **488,** 185–188 (2012).
18. Ma, X.-S. *et al.* Quantum teleportation over 143 kilometres using active feed-forward. *Nature* **489,** 269–273 (2012).
19. Stevenson, R. *et al.* Quantum teleportation of laser-generated photons with an entangled-light-emitting diode. *Nature Commun.* **4,** 2859 (2013).
20. Bussières, F. *et al.* Quantum teleportation from a telecom-wavelength photon to a solid-state quantum memory. *Nature Photon.* **8,** 775–778 (2014).
21. Pfaff, W. *et al.* Unconditional quantum teleportation between distant solid-state quantum bits. *Science* **345,** 532–535 (2014).
22. Wang, X.-L. *et al.* Quantum teleportation of multiple degrees of freedom of a single photon. *Nature* **518,** 516–519 (2015).
23. Takesue, H. *et al.* Quantum teleportation over 100 km of fiber using highly efficient superconducting nanowire single-photon detectors. *Optica* **2,** 832–835 (2015).
24. Ren, J.-G. *et al.* Long-distance quantum teleportation assisted with free-space entanglement distribution. *Chin. Phys. B* **18,** 3605–3610 (2009).
25. Barz, S. *et al.* Demonstration of blind quantum computing. *Science* **335,** 303–308 (2012).
26. Yang, T. *et al.* Experimental synchronization of independent entangled photon sources. *Phys. Rev. Lett.* **96,** 110501 (2006).
27. Kaltenbaek, R., Blauensteiner, B., Żukowski, M., Aspelmeyer, M. & Zeilinger, A. Experimental interference of independent photons. *Phys. Rev. Lett.* **96,** 240502 (2006).
28. Brendel, J., Gisin, N., Tittel, W. & Zbinden, H. Pulsed energy-time entangled twin-photon source for quantum communication. *Phys. Rev. Lett.* **82,** 2594–2597 (1999).
29. Hoeffding, W. Probability inequalities for sums of bounded random variables. *J. Am. Stat. Assoc.* **58,** 13–30 (1963).
30. Valivarthi, R. *et al.* Quantum teleportation across a metropolitan fibre network. *Nat. Photon.* http://dx.doi.org/10.1038/nphoton.2016.180 (2016).

Acknowledgements

We are grateful to the staff of the QuantumCTek. We thank Y. Liu, H. Lu, P. Xu, Y.-P. Wu, Y.-L. Tang, X. Ma, X. Xie, Y.-A.C. and C.-Z.P. for discussions, and C. Liu for helping with artwork design. This work was supported by the National Fundamental Research Program (under Grant No. 2013CB336800), the National Natural Science Foundation of China, the Chinese Academy of Science.

Author contributions

Q.Z. and J.-W.P. conceived and designed the experiments, S.-J.C., W.-J.Z., S.M., T.Y., H.T., L.-X.Y. and Z.W. fabricated and characterized the SNSPDs, Q.-C.S. and W.Z. designed and characterized the photon sources, Q.-C.S., Y.-L.M. and Y.-F.J. carried out the field test, X.J.,T.-Y.C. and X.-F.C. provided experimental assistance, Q.-C.S., Y.-B.Z. and J.-Y.F. analysed the data, Q.-C.S., X.-F.C., J.-Y.F., Q.Z. and J.-W.P. wrote the manuscript with input from all authors and Q.Z. and J.-W.P. supervised the whole project.

Additional information

Supplementary information is available in the online version of the paper. Reprints and permissions information is available online at www.nature.com/reprints. Correspondence and requests for materials should be addressed to Q.Z. and J.-W.P.

Competing financial interests

The authors declare no competing financial interests.

Methods

Quantum-state preparation. Charlie first modulates the CW laser beam ($\lambda = 1552.54$ nm) emitted by a distributed feedback laser (DFB) into 75 ps pulses with an EOM at a repetition frequency of 100 MHz. After passing the laser pulses through an unbalanced Mach–Zehnder interferometer (MZI) with a path difference of 1 ns, Charlie amplifies the generated sequence of two consecutive pulses with an erbium-doped fibre amplifier (EDFA) and then feeds them into a 300 m dispersion shifted fibre (DSF) to generate time-bin entangled photon pairs through an FWM process. The DSF is immersed in liquid nitrogen to reduce phonon-related single-photon noise. Charlie uses a filter system composed of cascaded dense wavelength division multiplexing (DWDM) devices to select paired signal (1549.36 nm) and idler (1555.73 nm) photons with the pump light attenuated by 115 dB. The quantum state of the time-bin entangled photon pairs is $|\Phi^+\rangle_{si} = 1/\sqrt{2}(|t_0\rangle_s|t_0\rangle_i + |t_1\rangle_s|t_1\rangle_i)$.

Alice prepares the input quantum state, $|\psi\rangle_{in} = 1/\sqrt{2}(|t_0\rangle_{in} + e^{i\theta}|t_1\rangle_{in})$, by passing the heralded single photons through an unbalanced MZI with a path difference of 1 ns, where the phase θ can be tuned by varying the temperature of the MZI. She prepares the input states, $|t_0\rangle_{in}(|t_1\rangle_{in})$, by replacing the MZI with a segment of fibre with an effective delay equal to the short (long) arm of the MZI.

Bell-state discrimination. Charlie performs the BSM using a fibre BS tree and four SNSPDs (the 40 ns recovery time prohibits SNSPD to detect the photons in two consecutive time bins). The two input photons meet at the first BS to form a superposition of four Bell states. The Bell state $|\Psi^-\rangle$ distinguishes itself by having the two photons leaving at separate ports of the BS. By passing photons through the second BS in the fibre BS tree, we can identify the Bell state $|\Psi^+\rangle$ with 50% of success by positioning the first time bin in one clock cycle and the second time bin in the next clock cycle of the FPGA which is synchronized with the master clock at 200 MHz.

Quantum-state tomography and process tomography. In a two level system, the density matrix can be written as

$$\rho = \frac{1}{2}\left(I + \sigma_x\frac{S_1}{S_0} + \sigma_y\frac{S_2}{S_0} + \sigma_z\frac{S_3}{S_0}\right) \tag{2}$$

where S_i ($i = 0, 1, 2, 3$) are the four Stokes parameters, which can be obtained as the following using the photon counts n_0, n_1, n_D, n_A, n_R, and n_L of the projection measurements on states t_0, t_1, D, A ($|A\rangle = 1/\sqrt{2}(|t_0\rangle - |t_1\rangle)$), R and L ($|L\rangle = 1/\sqrt{2}(|t_0\rangle - i|t_1\rangle)$), respectively.

$$\begin{aligned} S_0 &= n_0 + n_1 \\ S_1 &= n_D - n_A \\ S_2 &= n_R - n_L \\ S_3 &= n_0 - n_1 \end{aligned} \tag{3}$$

We implement the six projection measurements by using an unbalanced MZI with a path difference of 1 ns. After passing through the MZI, the photons can be observed in three consecutive time bins. The arrival times of the feedforward signal and the photodetection signal from the two SNSPDs are recorded with a TDC for coincidence measurements (which corresponds to a fourfold coincidence detection on the two-photon pairs originally created by Alice and Charlie). The detections in first time bin and the third time bin correspond to projection measurement on the time basis $\{|t_0\rangle, |t_1\rangle\}$, whereas that in the second time bin corresponds to projection measurement on the energy basis $\{1/\sqrt{2}(|t_0\rangle + e^{i\theta}|t_1\rangle), 1/\sqrt{2}(|t_0\rangle - e^{i\theta}|t_1\rangle)\}$, where the phase θ can be tuned by adjusting the temperature of the MZI. We implement projection measurements on two non-orthogonal bases $\{|D\rangle, |A\rangle\}$ and $\{|R\rangle, |L\rangle\}$ by setting the phase of the MZI as 0 and $\pi/2$, respectively[23]. In each projection measurement on an energy basis, the projection measurement on a time basis is implemented simultaneously. We reconstruct the density matrices ρ by applying a maximum likelihood estimation on the raw data. The state fidelities of the teleported quantum states are calculated with the reconstructed density matrices via relation $F = {}_{fin}\langle\psi|\rho|\psi\rangle_{fin}$. The uncertainties in state fidelities extracted from these density matrices are calculated using a Monte Carlo routine assuming Poissonian errors.

The process of a quantum-teleportation operation may be examined by quantum-process tomography. The relation between the input quantum state ρ and the output quantum state $\varepsilon(\rho)$ can be described as $\mathcal{E}(\rho) = \sum_{m,n=1}^{4}\chi_{mn}E_m\rho E_n^\dagger$, where $E_m \in \{I, \sigma_x, \sigma_y, \sigma_z\}$. The process matrix χ contains all information about the mapping relation between the input quantum state and output quantum state. In one qubit case, the process matrix can be determined using the results of quantum-state tomography for input states t_0, t_1, D and R (ref. 2). In an ideal case for our experiment, the process matrix, χ_{ideal}, has only one non-zero component, χ_{33}, which means the output quantum state is the input quantum state on a unitary operation σ_z. The process fidelity is calculated as $F_{proc} = \mathrm{Tr}(\chi_{ideal}\chi)$, which should be related to the average fidelity by $\bar{F} = (2F_{proc} + 1)/3$.